Synthesis of shape-controlled $ZnSn(OH)_6$ and gas sensing properties

HAN Lixian[1], DU Mengjuan[1], LI Yusheng[1], YE Bin[2], YU Xibin[1*]

(1. College of life and Environment Sciences, Shanghai Normal University, Shanghai 200234, China;
2. Department of Applied Mathematics, Shanghai University of Finance and Economics, Shanghai 200433, China)

Abstract: Monodisperse $ZnSn(OH)_6$ (ZHS) microcrystallites (MCs) with two morphologies have been prepared through a facile preparation method without complicated steps, advanced experimental conditions or equipments. The morphology and compositional characteristics of the 3D hierarchitectures (HAs) of ZHS MCs were investigated by various techniques such as XRD, FESEM, TEM, UV-vis spectra, BET. In the reaction system the morphology evolution from cube to sphere was controlled with adding different concentration of NH_4OH. The gas sensors based on ZHS exhibited a good gas sensitivity to HCHO. However, the gas sensors based on spherical ZHS MCs exhibited the higher sensitivity, shorter recovery time and good reproducibility to HCHO than those of cubic ZHS MCs. More importantly, it was found that spherical ZHS MCs with ~600 nm size had the best gas-sensing properties owing to more oxygen vacancy defects, less band gap energy, and larger active surface area.

Key words: ZHS; TEM; vacancy defects; less band gap energy

CLC number: O 611.64 **Document code:** A **Article ID:** 1000-5137(2013)01-0065-08

1 Introduction

The fabrication of nano-or micro-size particles with controlling morphologies, orientations, and dimensionalities has attracted much attention, because the physical and chemical properties of materials can be strongly influenced by their sizes and shapes [1-11]. The study of composite metal oxides (CMOs) is always interesting to researchers because their performances are superior over single metal oxides in many cases [12-13], such as gas-sensor materials. For instance, polyhedral zinc hydroxystannate (ZHS), $CdIn_2O_4$ [14] and $EuFeO_3$ nanoparticles have been used as gas-sensor materials [15].

Zinc hydroxystannate (ZHS), an important member of CMOs, is a kind of perovskite structure tending to form face-centered-cubic (FCC) crystal structure. Up to now, zinc hydroxystannate has been widely used as fire retardant and smoke inhibitor, photocatalyst, inorganic filler, and flame-retardant [15-18]. Furthermore, ZHS thermal decomposition products including $ZnSnO_3$ [19-20], crystalline SnO_2 and Zn_2SnO_4 can be used in lithium

Received date: 2012-11-20

Foundation item: This work is supported by the Shanghai Science & Technology committee (12521102501, 11ZR1426500), the first-class discipline construction planning in Shanghai University, the Program of Shanghai Normal University (DZL124).

Biography: HAN Lixian (1988-), female, graduate student, College of Life and Environment Sciences, Shanghai Normal University; YU Xibin (1956-), male, professor, College of Life and Environment Sciences, Shanghai Normal University.

* Corresponding author

© 1994-2013 China Academic Journal Electronic Publishing House. All rights reserved. http://www.cnki.net

ion battery anodes, gas sensors and photocatalysts [19-20].

Nano-microparticles of ZHS with different shapes such as nanocage, 14-faceted polyhedra, and wire-like have been synthesized by various synthesis routes, including thermal decomposition [21] hydrothermal synthesis [22-23] low temperature ion exchange [24] and different surfactants have assisted wet-chemical methods at low temperature [25]. However, the synthesis strategies mentioned above usually need complex operating procedures, expensive raw materials and further heat treatment. Considering their excellent features, such as high sensitivity, short recovery time and good reproducibility, a novel route is highly required for the fabrication of the hierarchical architectures assembled with nanostructured building blocks of ZHS. So far, the preparations of ZHS through low-cost, convenient routes are still a challenge. In addition, to our knowledge, the shape-controlled synthesis and the gas sensing investigation of ZHS MCs with different shapes and a facile method have not been reported, especially ZHS MCs self-assembled by nanoparticles.

Herein, we demonstrate that different shapes of ZHS(microcube, microsphere) with uniform size could be on a large scale through precipitation process. It is worthy to note that neither complicated steps nor advanced experimental conditions or equipments were used, making this process easy. Then, the formation mechanisms of the ZHS crystallites were studied via a series of time-dependent experiments. In the following section, UV-vis absorption spectra have been used to discuss the influences of gas sensor based on ZHS MCs including oxygen vacancy defects, the gas adsorption, band gap energy, and active surface area. However, the band gap energy of spherical ZHS crystallites was less than that of nanocubic crystallites. It is clearly that the sensors based on spherical ZHS MCs exhibited faster response, higher sensitivity, and shorter recovery times toward HCHO gas than those based on ZHS nancubic ZHS because of more oxygen vacancy defects, less band gap energy, and larger active surface area. The as-prepared MCs should be significant for exploiting new gas-sensing materials in the future.

2 Experimental Section

2.1 Materials

All reagents were analytic grade from Aladdin reagent(China) Co., LtdS. and used as received without further purification. Deionized Water(PURELAB Plus, PALL) with a resistivity of 18 M? cm was used throughout.

2.2 Preparation of ZHS Cubic Crystallites

In a typical experiment, 2.8754 g(10 mmol) of zinc sulfate heptahydrate($ZnSO_4 \cdot 7H_2O$) was added into 100 mL of deionized water(DW), and the solution was stirred at room temperature until $ZnSO_4 \cdot 7H_2O$ was dissolved completely. Then appropriate sodium stannate trihydrate($Na_2SnO_3 \cdot 3H_2O$) solution was dropped into $ZnSO_4 \cdot 7H_2O$ solution, making the molar ration of [Zn] / [Sn] = 1∶1. After the completion of the above steps, the mixed solution was stirred for 5 h. After the reaction, the precipitates were collected by centrifugation, washed with DW for several times to remove residual ions in the products. The final products were then dried in air at 100 ℃ for 8 h before characterization.

2.3 Preparation of ZHS Spherical Crystallites

Before adding $Na_2SnO_3 \cdot 3H_2O$ solution, the adequate ammonia was dropped into the $ZnSO_4$ solution. The other synthesizing process was the same as the preparation of ZHS nanocubic crystallites.

© 1994-2013 China Academic Journal Electronic Publishing House. All rights reserved. http://www.cnki.net

2.4 General Characterization

X-ray powder diffraction (XRD) pattern was recorded using a Japan Regaku D/max cA X-ray diffractometer equipped with graphite monochromatized Cu Kα radiation ($\lambda = 1.5418$ Å) irradiated with a scanning rate of 4 deg/min. The Field-emission scanning electron microscopic (FESEM) images were obtained using a JEOL JSM-7500F microscope operated at an acceleration voltage of 15 kV. A JEOL JEM-200CX microscope operating at 160 kV in the bright-field mode was used for Transmission Electron Microscopy (TEM). Selected area electron diffraction (SAED) pattern was performed on a JEOL JEM-2010 electron microscope operating at 200 kV.

2.5 Measurements of gas-sensing

The gas-sensing properties were measured using a static test system of WS-60A made by Hanwei Electronics Co. Ltd., Henan Province, China. The sensors were fabricated by a modifying method described in the reference [20]. Before the sensitivity measurement, the samples were connected to the 5 V dc source and the heat voltage was maintained at 5 V till the stabilization of the base line voltage.

In our gas-sensing measurements, a given amount of test gas was injected into a closed chamber, and the sensor was put into the chamber for the measurement of the sensitive performance. After each measurement, the sensor was exposed to the atmospheric air by opening the chamber. Sensitivity was defined as $S = R_a/R_g$, where R_a was the average resistance in air and R_g was the average resistance in the test gas. The response and recovery time were defined as the time taken by the sensor to achieve 90% of the total resistance change in the case of adsorption and desorption, respectively.

3 Results and Discussion

3.1 Structural Characterization

The composition and phase purity of the as-obtained products are first examined by X-ray powder diffraction (XRD) patterns. Fig. 1 shows the XRD patterns of typical ZHS with microcube (a) and microsphere (b), respectively. The XRD patterns of the ZHS powders are quite similar. All of the diffraction peaks can be indexed to the standard ZHS with the perovskite structure (JCPDS No. 20 - 1455), confirming that the as-synthesized samples have a typical FCC crystal structure. According to data of XRD, the lattice parameters calculated via the XRD data for ZHS microcube and microsphere are corresponding to 7.7656 Å and 7.7456 Å, respectively. Peaks at around 22.8, 40.2, and 52.6 correspond to the (200), (220), and (420) planes of the as-obtained products. By comparison, the diffraction peak intensity of sphereical product is stronger than that of microcube. No impurity phases are detected from the XRD pattern, indicating that two types ZHS crystallites with high purity could be obtained under current synthetic conditions.

3.2 Morphology Characterization

Many researchers have reported ZHS structures with different morphologies could be obtained hydrothermally under appropriate reaction conditions [22-23]. In this work, the microcube ZHS crystallites were obtained simply by the reaction between $ZnSO_4 \cdot 7H_2O$ and $Na_2SnO_3 \cdot 3H_2O$, while the spherical ZHS MCs were obtained by introducing NH_4OH into the reaction system.

The morphology and structure details of the as-obtained ZHS products are investigated by SEM, FESEM, and TEM techniques. It can be clearly seen from Fig. 2A that the ZHS products are entirely composed of a large-scale

© 1994-2013 China Academic Journal Electronic Publishing House. All rights reserved.　http://www.cnki.net

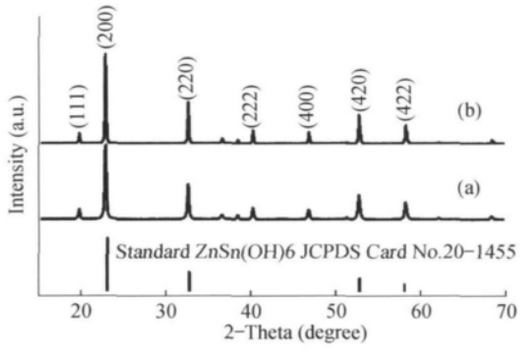

Figure 1 XRD patterns of the as-prepared ZHS products: nanocube(a), nanosphere(b) and Standard XRD pattern of ZHS(JCPDS No. 20 - 1455)

of uniform and monodisperse MCs. High-magnification FESEM image(Fig. 2B) shows that the products consist of homogeneous nanocubes with side lengths of about 500 - 600 nm. A representative TEM micrograph of cubic ZHS crystallites is shown in Fig. 2C, clearly showing that the single nanoparticle has perfect cubic profile with very clear edges and corners. The corresponding selected area electron diffraction(SAED) pattern of cubic crystallites(as shown in Fig. 2D) confirms that the nanocubes have good crystallinity and there is no secondary phase. The corresponding selected area electron diffraction(SAED) pattern of cubic crystallites(as shown in Fig. 2D) confirms that the nanocubes have well-crystallized structure. The diffraction spots of the typical FCC crystal structure could be indexed to {020}, {220} and {200} panels of the $ZnSn(OH)_6$ (ZHS) microcrystallites.

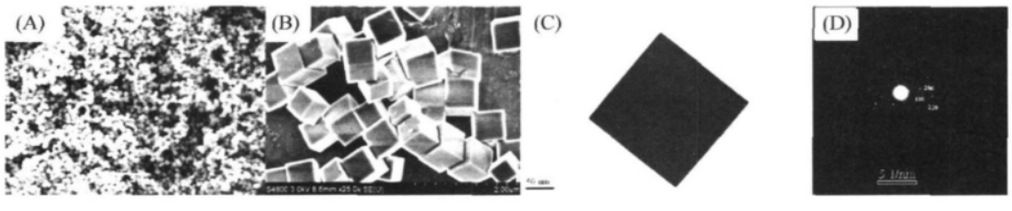

Figure 2 SEM, TEM and SAED images of the ZHS nanocubic crystallites: (A) low magnification SEM image; (B) high magnification FESEM image; (C) high magnification TEM image; (D) SAED pattern

In the further process, spherical ZHS MCs were obtained with adding appropriate amount of ammonia in the reaction solution. Fig. 3A shows the panoramic morphologies of the typical sample. The results indicate that the product consists of monodisperse spherical crystallites with glossy surface in the size range of 500 ~ 600 nm. HoweverF, high magnification FESEM images(Fig. 3B and 3C) display that the as-obtained spherical ZHS crystallite is not as smooth as the former shown(Fig. 3A). A clear grain boundary can be observed on the surface of ZHS microspheres(Fig. 3B and C), indicating that the as-obtained spherical ZHS crystallites are constituted by the oriented aggregation of small ZHS nanoparticles. More structure information of spherical ZHS crystallites is researched by TEM. As shown in high magnification TEM images(Fig. 3C), the surface of the as-obtained ZHS spherical crystallites is rough. Many nanoparticles attach on the surface of ZHS microspheres. It also demonstrates the as-obtained spherical ZHS crystallites are composed of small ZHS nanoparticles with diameter of 5 ~ 10 nm diameter, which validates the observation results of FESEM tests(Fig. 3B). The selected area electron diffraction

© 1994-2013 China Academic Journal Electronic Publishing House. All rights reserved. http://www.cnki.net

(SAED) pattern (Inset Fig. 3C) taken from the edge of the sphere marked by a circle exhibits the clear diffraction lattices, revealing the single-crystalline nature of the sample with a preferential grown direction. The diffraction spots could also be indexed to {020}, {220}, and {200} panels of the $ZnSn(OH)_6$ (ZHS) microcrystallites.

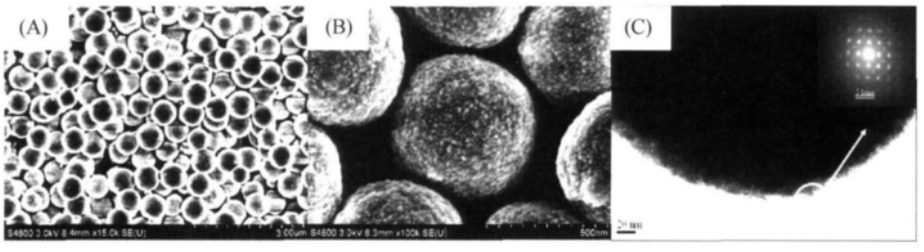

Figure 3　SEM and TEM images of the spherical ZHS MCs: (A) low magnification FESEM image; (B) high magnification FESEM image; (C) high magnification TEM image, inset in (C) SAED pattern

3.3　Optical Absorption and BET

The optical absorption properties of ZHS MCs semiconductor were measured by The UV-vis absorption spectra. As shown in Fig. 4, the E_g of two samples are 5.02eV (microcube) and 4.90eV (microsphere) which are calculated on the basis of the corresponding absorption edges. This indicates that the spherical ZHS MCs have less band gap energy, which may help the O_2 adsorption on the ZHS surface to trap electrons from the conduction band of ZHS and enhance the sensing performance. The surface area of these morphologies are shown in the Table 1. The surface area of spherical ZHS MCs is larger than that of the microcubic shape (as shown in Table 1). It is reported that "surface accessibility" becomes one of crucial factors to maintain the high sensitivity of the gas sensor[26]. Hence, the sensor based on spherical ZHS MCs should exhibit higher sensitivity.

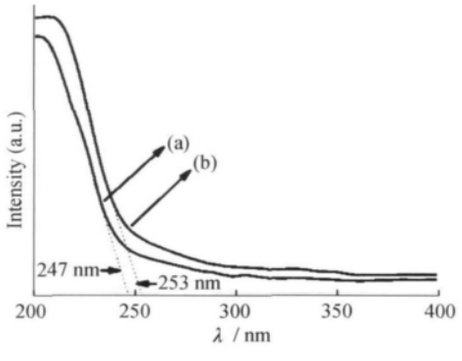

Figure 4　The UV-visible absorption spectrum of (a) nanocube and (b) nanosphere samples

Table 1　Active surface srea of ZHS MCs

Mean Shape	mean particle size (nm)	surface area (m^2/g)
sphere	~600	54.9
cubic	~600	36.4

3.4　Gas sensor performance

According to the sensing mechanism of Wolkenstein's model for semiconductors[27], when the sensors are

© 1994-2013 China Academic Journal Electronic Publishing House. All rights reserved.　http://www.cnki.net

exposed to air, the surface of ZHS sensors could adsorb oxygen species to ionize into O^-(ads) or O^{2-}(ads). This is because oxygen atom owns the strong electronegativity from the conduction band of ZHS. Hence, the concentration of electrons in the conduction band would decrease and the resistance of the material would increase. And then a chemical reaction would take place between HCHO and O^{2-}(ads), which leads to a relatively strong activation on the surface of the ZHS:

$$HCHO(gas) + O^{2-}(ads) \rightarrow H_2O(g) + CO_2(g) + 2e^- .$$

As to say, the oxygen vacancy, the band gap energy, and the active surface area may have affects on the gas sensor. spherical ZHS MCs may present better gas sensor performance compared with cubic ZHS MCs, because spherical ZHS MCs have more oxygen vacancy, less band gap energy, and larger BET surface area.

Gas sensor performance based on ZHS MCs to HCHO with the similar size of microcube(line a) and microsphere(line b) are Shown in the Fig. 5. The typical response curves of ZHS-based gas sensors with different shapes to increasing concentration of HCHO are shown in the Fig. 5A. It is obvious that the sensitivity of gas sensors increases rapidly with the increase of HCHO concentrations, revealing that the sensitivities of the ZHS-based gas sensors are excellent to HCHO. But the sensitivity of the spherical ZHS MCs increases faster than that of the cubic MCs with the same response time and the same HCHO concentration.

As shown in Fig. 5B, it is clear that ZHS based sensors have a wide detection range for HCHO(from 10 to 100 ppm). The sensitivity of the spherical ZHS MCs especially increases faster with the same concentration of HCHO. At the same time, the recovery time of sensor based on spherical ZHS sphere MCs is shorter. Hence, the sensors based on spherical ZHS MCs are much more sensitive than those based on ZHS cubic MCs. The detection limit of the as-prepared ZHS sensors can reach as low as several parts per million for HCHO. Meanwhile, the recovery time of sensor based on spherical ZHS sphere MCs is the shortest.

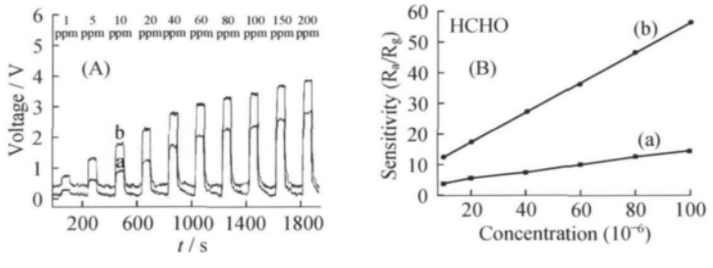

Figure 5 (A) Sensitivities of the sensors based on ZHS MCs with different shapes to increased concentrations of HCHO. (B) Typical response curves of ZHS NCs sensors of different shapes to HCHO with increasing concentrations. In parts A and B, (a) and (b) correspond to the ZHS NCs of nanocube and nanosphere, respectively

4 Conclusion

In conclusion, the successful synthesis of uniform ZHS MCs with different shapes via a facile process was proposed. It was found that the micro-cube morphology evolved to microsphere with adding different concentrations of NH_4OH. The gas sensors based on both of the two morphologies exhibited good sensor performance toward HCHO gas. The sensor based on spherical ZHS MCs demonstrated faster response, higher sensitivity and shorter recovery time owing to more oxygen vacancy defects, less band gap energy, and larger

© 1994-2013 China Academic Journal Electronic Publishing House. All rights reserved. http://www.cnki.net

active surface area. The as-synthesized ZHS MCs make them ideal candidates for HCHO gas-sensing devices.

References:

[1] PENG X G, MANNA L, YANG W D, et al. Shape control of CdSe nanocrystals [J]. Nature, 2000, 404: 59 – 61.

[2] BUDAI J D, WHITE C W, WITHROW S P, et al. Controlling the size, structure and orientation of semiconductor nanocrystals using metastable phase recrystallization [J]. Nature, 1997, 390: 384 – 386.

[3] COZZOLI P D, MANNA L, CURRI M L, et al. Shape and phase control of colloidal ZnSe nanocrystals [J]. Chemistry of Materials, 2005, 17(6): 1296 – 1306.

[4] GONG Q, QIAN X, CAO H, et al. Novel shape evolution of $BaMoO_4$ microcrystals [J]. The Journal of Physical Chemistry B, 2006, 110(39): 19295 – 19299.

[5] TIAN Y, LIU H, ZHAO G, et al. Shape-controlled electrodeposition of gold nanostructures [J]. The Journal of Physical Chemistry B, 2006, 110(46): 23478 – 23481.

[6] FANG X, BANDO Y, YE C, et al. Shape-and size-controlled growth of ZnS nanostructures [J]. The Journal of Physical Chemistry C, 2007, 111(24): 8469 – 8474.

[7] NANDWANA V, ELKINS K E, POUDYAL N, et al. Size and shape control of monodisperse FePt nanoparticles [J]. The Journal of Physical Chemistry C, 2007, 111(11): 4185 – 4189.

[8] TAN T T, SELVAN S T, ZHAO L, et al. Size control, shape evolution, and silica coating of near-infrared-emitting PbSe quantum dots [J]. Chemistry of Materials, 2007, 19(13): 3112 – 3117.

[9] WANG F, TANG R, YU H, et al. Size-and shape-controlled synthesis of bismuth nanoparticles [J]. Chemistry of Materials, 2008, 20(11): 3656 – 3662.

[10] ZHANG H, XU J J, CHEN H Y. Shape-controlled gold nanoarchitectures: synthesis, superhydrophobicity, and electrocatalytic properties [J]. The Journal of Physical Chemistry C, 2008, 112(36): 13886 – 13892.

[11] BAO N, SHEN L, AN W, et al. Formation mechanism and shape control of monodisperse magnetic $CoFe_2O_4$ nanocrystals [J]. Chemistry of Materials, 2009, 21(14): 3458 – 3468.

[12] WHITBY R L D, BRIGATTI K S, KINLOCH I A, et al. Novel Mg_2SiO_4 structures [J]. Chemical Communications, 2004 (21): 2396 – 2397.

[13] ZHANG T, JIN C G, QIAN T, et al. Hydrothermal synthesis of single-crystalline $La_{0.5}Ca_{0.5}MnO_3$ nanowires at low temperature [J]. Journal of Materials Chemistry, 2004, 14: 2787 – 2789.

[14] MAHANUBHAV M D, PATIL L A. Studies on gas sensing performance of CuO-modified $CdIn_2O_4$ thick film resistor [J]. Sensors and Actuators B: Chemical, 2007, 128(1): 186 – 192.

[15] SIEMONS M, SIMON U. High throughput screening of the propylene and ethanol sensing properties of rare-earth orthoferrites and orthochromites [J]. Sensors and Actuators B: Chemical, 2007, 126(1): 181 – 186.

[16] YANG L, HU Y, YOU F, et al. A novel method to prepare zinc hydroxystannate-coated inorganic fillers and its effect on the fire properties of PVC cable materials [J]. Polymer Engineering & Science, 2007, 47(7): 1163 – 1169.

[17] ZHANG B, JIAO Y, XU J Z. A study on the flame-retardance of poly(vinyl chloride) incorporated with metal hydroxystannates [J]. Journal of Applied Polymer Science, 2009, 112(1): 82 – 88.

[18] FU X, WANG X, DING Z, et al. Hydroxide $ZnSn(OH)_6$: A promising new photocatalyst for benzene degradation [J]. Applied Catalysis B: Environmental, 2009, 91(1 – 2): 67 – 72.

[19] RONG A, GAO X P, LI G R, et al. Hydrothermal synthesis of Zn_2SnO_4 as anode materials for Li-ion battery [J]. The Journal of Physical Chemistry B, 2006, 110(30): 14754 – 14760.

© 1994-2013 China Academic Journal Electronic Publishing House. All rights reserved.　http://www.cnki.net

[20] ZHANG W H, ZHANG W D. Fabrication of SnO_2 – ZnO nanocomposite sensor for selective sensing of trimethylamine and the freshness of fishes [J]. Sensors and Actuators B: Chemical, 2008, 13(2): 403 – 408.

[21] WROBEL G, PIECH M, DARDONA S, et al. Seedless synthesis and thermal decomposition of single crystalline zinc hydroxystannate cubes [J]. Crystal Growth & Design, 2009, 9(10): 4456 – 4460.

[22] ZHANG Y, GUO M, ZHANG M, et al. Hydrothermal synthesis and characterization of single-crystalline zinc hydroxystannate microcubes [J]. Journal of Crystal Growth, 2007, 308(1): 99 – 104.

[23] FAN H, AI S, JU P. Room temperature synthesis of zinc hydroxystannate hollow core-shell microspheres and their hydrothermal growth of hollow core-shell polyhedral microcrystals [J]. Cryst Eng Comm, 2011, 13: 113 – 117.

[24] KOVACHEVA D, PETROV K. Preparation of crystalline $ZnSnO_3$ from Li_2SnO_3 by low-temperature ion exchange [J]. Solid State Ionics, 1998, 109(3 – 4): 327 – 332.

[25] WANG L, TANG K, LIU Z, et al. Single-crystalline $ZnSn(OH)_6$ hollow cubes via self-templated synthesis at room temperature and their photocatalytic properties [J]. Journal of Materials Chemistry, 2011, 21: 4352 – 4357.

[26] GENG B, FANG C, ZHAN F, et al. Synthesis of Polyhedral $ZnSnO_3$ Microcrystals with Controlled Exposed Facets and Their Selective Gas-Sensing Properties [J]. Small, 2008, 4(9): 1337 – 1343.

[27] HAICK H, AMBRICO M, LIGONZO T, et al. Controlling semiconductor/metal junction barriers by incomplete, nonideal molecular monolayers [J]. Journal of the American Chemical Society, 2006, 128(21): 6854 – 6869.

不同形貌的 $ZnSn(OH)_6$ 的制备与气敏性能的应用

韩丽仙[1], 杜孟娟[1], 李宇生[1], 叶 斌[2], 余锡宾[1*]

(1. 上海师范大学 生命与环境科学学院, 上海 200234; 2. 上海财经大学 应用数学系, 上海 200433)

摘 要: 使用简易的流程, 实验条件或设备, 简单的制备方法制备出两种形貌的单分散 $ZnSn(OH)_6$(ZHS)微晶(MCs). 利用 X 射线衍射(XRD), 场发射电子显微镜(FESEM), 透射电子显微镜(TEM), 紫外可见吸收光谱(UV – Vis), 比表面吸附(BET)等不同的测试手段对羟基锡酸锌(ZHS)微晶(MCs)的三维多级纳米结构(HAs)的形貌和结构进行了表征. 通过控制所滴加氨水的浓度, 反应体系中羟基锡酸锌的形貌可由立方形转变为球形. 以羟基锡酸锌为气敏材料的传感器对甲醛有较好的气敏性. 然而, 和立方形羟基锡酸锌微晶相比, 球形羟基锡酸锌微晶对甲醛表现出更高的灵敏度, 更快的响应速度和良好的重现性. 更重要的是, 由于球形羟基锡酸锌微晶具有更多的氧空位缺陷, 较小的带隙能和较大的活性表面积, 球形羟基锡酸锌在 600 nm 左右表现出最优异的气敏性能.

关键词: 羟基锡酸锌; 透射电子显微镜; 空位缺陷; 低带隙能

(责任编辑: 郁 慧)

© 1994-2013 China Academic Journal Electronic Publishing House. All rights reserved. http://www.cnki.net